International Journal of Pharmaceutics 532 (2017) 185–193

Contents lists available at ScienceDirect

International Journal of Pharmaceutics

journal homepage: www.elsevier.com/locate/ijpharm

Modelling the primary drying step for the determination of the optimal dynamic heating pad temperature in a continuous pharmaceutical freeze-drying process for unit doses

Laurens De Meyer[a], Joris Lammens[c], Séverine Thérèse F.C. Mortier[b,a], Brecht Vanbillemont[a], Pieter Jan Van Bockstal[a], Jos Corver[a], Ingmar Nopens[b], Chris Vervaet[c], Thomas De Beer[a,*]

[a] Laboratory of Pharmaceutical Process Analytical Technology, Department of Pharmaceutical Analysis, Faculty of Pharmaceutical Sciences, Ghent University, Ottergemsesteenweg 460, 9000 Ghent, Belgium
[b] BIOMATH, Department of Mathematical Modelling, Statistics and Bioinformatics, Faculty of Bioscience Engineering, Ghent University, Coupure Links 653, 9000 Ghent, Belgium
[c] Laboratory of Pharmaceutical Technology, Department of Pharmaceutics, Faculty of Pharmaceutical Sciences, Ghent University, Ottergemsesteenweg 460, 9000 Ghent, Belgium

ARTICLE INFO

Keywords:
Continuous freeze-drying
Mathematical modelling
Conduction
NIR spectroscopy
Mechanistic modelling
Spin freezing

ABSTRACT

In the pharmaceutical industry, traditional freeze-drying of unit doses is a batch-wise process associated with many disadvantages. To overcome these disadvantages and to guarantee a uniform product quality and high process efficiency, a continuous freeze-drying process is developed and evaluated. The main differences between the proposed continuous freeze-drying process and traditional freeze-drying can be found firstly in the freezing step during which the vials are rotated around their longitudinal axis (spin freezing), and secondly in the drying step during which the energy for sublimation and desorption is provided through the vial wall by conduction via an electrical heating pad. To obtain a more efficient drying process, the energy transfer has to be optimised without exceeding the product and process limits (e.g. cake collapse, choked flow). Therefore, a mechanistic model describing primary drying during continuous lyophilisation of unit doses based on conduction via heating pads was developed allowing the prediction of the optimal dynamic power input and temperature output of the electric heating pads. The model was verified by experimentally testing the optimal dynamic primary drying conditions calculated for a model formulation. The primary drying endpoint of the model formulation was determined via in-line NIR spectroscopy. This endpoint was then compared with the predicted model based endpoint. The mean ratio between the experimental and model based predicted drying time for six verification runs was 1.05 ± 0.07, indicating a good accordance between the model and the experimental data.

1. Introduction

In 2016, 50% of the by the FDA's Center for Drug Evaluation and Research (CDER) approved novel drugs were biopharmaceuticals (FDA, 2016). Many biopharmaceuticals are unstable in aqueous solution (Chi et al., 2003). The fact that approximately 50% of the approved biopharmaceutical drug products on the list of the Food and Drug Administration (FDA) and European Medicines Agency (EMA) are freeze-dried (lyophilised), indicates that freeze-drying is the preferred technology to stabilize these products (Costantino and Pikal, 2004).

Lyophilisation is a low temperature drying process, based on the principles of mass and heat transfer, employed to convert solutions of (heat) labile materials into solids having sufficient stability for distribution and storage (De Meyer et al., 2015).

Traditional freeze-drying is performed in three consecutive steps: freezing, primary drying and secondary drying (Wang, 2000; Pikal et al., 1983; Rey and May, 2010; Jennings, 1999). After aseptic filling of the formulation into the vials, they are positioned on the shelves of the freeze-dryer. During the freezing step, the temperature of the shelves is decreased to approximately −40 °C and most of the water in the formulation crystallizes into ice, thus concentrating the solutes which are in between the ice crystals (freeze-concentration). These solutes can

* Corresponding author.
E-mail addresses: Laurens.DeMeyer@UGent.be (L. De Meyer), Joris.Lammens@UGent.be (J. Lammens), Severine.Mortier@UGent.be (S.T.F.C. Mortier), Brecht.Vanbillemont@UGent.be (B. Vanbillemont), pieterjan.vanbockstal@ugent.be (P.J. Van Bockstal), Jos.Corver@RheaVita.nl (J. Corver), Ingmar.Nopens@UGent.be (I. Nopens), Chris.Vervaet@UGent.be (C. Vervaet), Thomas.DeBeer@UGent.be (T. De Beer).
URL: http://www.ugent.be/fw/pharmaceutical-analysis/en/research/pat (T. De Beer).

http://dx.doi.org/10.1016/j.ijpharm.2017.09.004
Received 13 June 2017; Received in revised form 1 September 2017; Accepted 2 September 2017
Available online 05 September 2017
0378-5173/

Nomenclature

ΔH_s	latent heat of ice sublimation (2838 J/g)
Δl	increase in dry product layer per time step t (m)
Δt	time step to calculate l (h)
$\dot{m}_{sub}$	sublimation rate (kg/h)
α	parameter describing K_v in function of P_c
β	parameter describing K_v in function of P_c
γ	adiabatic constant for triatomic gas (–)
ϕ	volume fraction of ice (–)
ρ_{ice}	density of ice (kg/m^3)
A_p	product area available for sublimation (m^2)
A_{Rp}	constant describing R_p in function of l (1/s)
B_{Rp}	constant describing R_p in function of l (1/m)
c	speed of sound for an ideal gas (m/s)
$d_{v,o}$	diameter of the vial opening (m)
h_f	height of the spin frozen product (m)
K_v	heat transfer coefficient (J/m^2 s K)
M	molecular weight of water (0.018015 kg/mol)
P_c	chamber pressure (Pa)
P_{sub}	power required for ice sublimation (W)
$P_{w,c}$	partial water vapour pressure in the drying chamber (Pa)
$P_{w,i}$	vapour pressure at the sublimation front (Pa)
R	gas constant (8.3144621 J/(mol K))
R_p	dry product mass transfer resistance (m/s)
$R_{p,0}$	constant describing R_p in function of l (m/s)
$r_{p,i}$	radius from the centre of the vial to the border of the spin frozen layer (m)
$r_{v,i}$	inner radius of the glass vial (m)
T_c	collapse temperature (K)
T_{eu}	eutectic temperature (K)
T_g'	glass transition temperature of the maximum freeze-concentrated formulation (K)
T_h	heating pad temperature (K)
T_i	product temperature at sublimation front (K)
T_p	product temperature (K)
T_{wv}	temperature of water vapour (K)
V	filling volume (m^3)
V_{max}	maximum volume of sublimed gas
$v_{sound,safe}$	safe velocity of sound (m/s)
$\dot{m}_{max}$	maximum sublimation rate (kg/s)

crystallize at the eutectic temperature (T_{eu}). If no crystallization occurs, the solutes concentrate until a glass is formed at the glass transition temperature of the maximally freeze-concentrated amorphous matrix (T_g') (Kasper and Friess, 2011). During primary drying, a vacuum, in general between 10 and 30 Pa, is introduced. Subsequently the temperature of the shelves is increased to supply the energy for sublimation. It is of utter importance to keep the product temperature at the sublimation front (T_i) below the collapse temperature (T_c) for an amorphous product or T_{eu} in case of a crystalline product during the entire primary drying process. The final step of the freeze-drying process is secondary drying where most of the unfrozen water is removed by desorption under deep vacuum and at an increased shelf temperature (Pikal, 2002).

Freeze-drying, as it is performed these days in the pharmaceutical industry, is a batch-wise process (Sarragua et al., 2010). Despite the increased importance of freeze-drying, indicated by the higher number of biopharmaceuticals, it is still an expensive and time-consuming process exhibiting several disadvantages such as the uncontrolled freezing step and uneven heat transfer in the freeze-drying chamber. The disadvantages of batch-wise freeze-drying have been extensively described in a previous paper from the authors (Kasper and Friess, 2011; Kauppinen et al., 2013; De Meyer et al., 2015). To overcome these disadvantages and to guarantee a uniform product quality, a continuous freeze-drying process has been developed.

The continuous freeze-drying process introduces two major differences compared to conventional batch freeze-drying. Firstly the freezing step, during which the vials are spun around their longitudinal axis, creating a thin frozen product layer at the vial wall (spin freezing) (Fig. 1). The solution is solidified by a flow of cold, sterile gas. The thinner product layer and larger surface area of the spin frozen product significantly contributes improving the efficiency of the freeze-drying process. The second major difference occurs in the drying step where energy is homogeneously supplied towards the vial wall either by conduction (e.g. electric heating pad) or radiation (e.g. infra-red heater) (De Meyer et al., 2015; Corver, 2013; Van Bockstal et al., 2017; Van Bockstal, 2017).

In the case of conductive drying, the energy can be provided by an electric heating pad which is wrapped around the vial creating a close contact between the vial and the heating pad for a homogeneous energy transfer (Fig. 2).

The continuous freeze-drying process is extensively described in previous work (De Meyer et al., 2015; Van Bockstal et al., 2017; Van Bockstal, 2017).

The most critical parameter during the primary drying step is T_i. To achieve an efficient freeze-drying process, T_i should be as high as possible during the primary drying step without exceeding T_c or T_{eu} for amorphous or crystalline materials, respectively. T_c is in general a few degrees higher than T_g' since the molecular motion at T_g' is sufficiently low to prevent viscous flow due to the high viscosity (Kasper and Friess, 2011). During secondary drying, the product temperature (T_p) should not exceed the glass transition temperature (T_g) to avoid cake collapse. Collapse is a loss of product structure, causing a poor cake appearance and possibly impeding the reconstitution of the dried product (Koganti et al., 2011; Jennings, 1999). If using constant freeze-drying settings (chamber pressure and energy input for drying), T_i would not be constant during the sublimation process because it depends on several parameters which continuously change during the process, e.g. the dried product mass transfer resistance (R_p) (Mortier et al., 2016). When the sublimation front is moving, a dried product layer is formed, leaving behind a network of pores which create a water vapour removal resistance (Konstantinidis et al., 2011). The continuous increase of the dried product layer (l) during sublimation also leads to a continuous increase in R_p. As a result, T_i at the sublimation interface will increase when a constant energy input and freeze-dryer chamber pressure is maintained for the whole drying trajectory.

However, in order to perform sublimation as efficient as possible, it

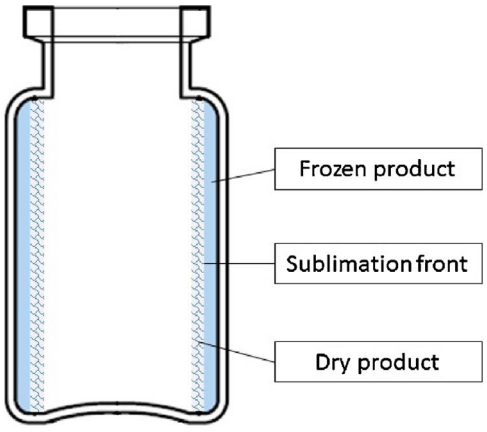

Fig. 1. schematic illustration of a spin frozen vial during the drying process.

Fig. 2. Spin frozen vial in close contact with surrounding electric heating pad.

is needed to keep T_i just below the T_c during the entire primary drying step. Therefore, the optimal combination of energy input and chamber pressure (P_c) is a dynamic combination during primary drying. A mechanistic model describing the primary drying step based on conductive heating, would allow the determination of the optimal combination of the heating pad temperature (T_h) and P_c, keeping the T_i as high as possible but still below the T_c during the entire sublimation process.

Compared to data-driven models, which are solely based on collected experimental data, mechanistic models are based on the underlying physics governing the process (Mortier et al., 2016). This research paper focuses on the mechanistic modelling of the primary drying step allowing the calculation of the optimal dynamic settings of the electric heating pads surrounding the vial and the chamber pressure during the continuous freeze-drying process.

2. Objectives

There are two objectives in this paper: (1) to develop a mechanistic model describing the primary drying process of spin frozen vials via conduction using electric heating pads. This model will allow calculating the optimal dynamic freeze-drying settings for the chamber pressure and the electric heating pad temperature during the primary drying step of the freeze-drying process for a model formulation. (2) To experimentally verify these calculated optimal dynamic freeze-drying settings for this model formulation.

3. Materials and methods

3.1. Development of a mechanistic model describing primary drying during continuous lyophilisation of unit doses based on conduction via electric heating pads

Primary drying consists of two phases. The equations describing primary drying are based on the principles of mass and energy transfer.

During the first part of the primary drying process, the pressure in the drying chamber is decreased until the desired chamber pressure (in this study) of 13.3 Pa is reached. Until that moment, the heating pads are turned off. The mass of ice which sublimed during the initial pressure decrease, due to energy from the surroundings, was experimentally determined (see further).

The second part of the primary drying process starts once the desired chamber pressure is reached and the heating pads are activated. During sublimation, the sublimation front moves towards the vial wall and the dried product layer increases in thickness. In traditional freeze-drying, a two-dimensional approach is necessary to model the primary drying step. In the case of continuous freeze-drying, a one-dimensional approach can be used as the product forms a conformal layer to the cylindrical vial wall. The end-effects at the bottom and top of the vial are excluded in the mechanistic model since the effect is small due to the small layer thickness.

When determining the maximum possible sublimation rate during primary drying, several limitations have to be taken into account.

The first limitation of the sublimation rate is the R_p of the formulation. Sublimation of the ice crystals creates a network of pores in the dried product. These pores create a resistance towards the water vapour generated at the sublimation front. When more water vapour is generated than the amount that can be transferred through the dried layer, the water vapour pressure at the sublimation front will increase. As the water vapour pressure is related to T_i (Eq. (5)), an uncontrolled increase of T_i is inevitable which can result in cake collapse.

The sublimation rate $\dot{m}_{\text{sub}}$ (kg/s) is given by:

$$\dot{m}_{\text{sub}} = A_p R_p (P_{w,i} - P_{w,c}) \tag{1}$$

with A_p the surface area of the spin frozen product (m^2), R_p the dry product resistance (m/s), $P_{w,i}$ the water vapour pressure above the sublimation front (Pa) and $P_{w,c}$ the partial water vapour pressure in the chamber (Pa). During primary drying, the composition of the gas in the drying chamber consists almost entirely of water vapour (Fissore et al., 2011). Therefore it is assumed that $P_{w,c}$ is equal to the overall pressure in the drying chamber. The surface area of the product during primary drying A_p is given by:

$$A_p = 2\pi h_f (r_{p,i} + l) \tag{2}$$

with h_f the height of the spin frozen product layer in the vial (m), l the dried layer thickness (m) and $r_{p,i}$ the radius from the centre of the vial to the border of the spin frozen layer (m), which is given by:

$$r_{p,i} = \sqrt{r_{v,i}^2 - \frac{V}{\pi h_f}} \tag{3}$$

with $r_{v,i}$ the inner vial radius (m), V the filling volume (m^3) and h_f the height of the spin frozen product layer (m).

R_p, another parameter in Eq. (1), depends on the thickness of the dried product layer l (m).

The following equation describes the link between R_p (m/s) and the dried layer thickness l (Fissore et al., 2009):

$$R_p = R_{p,0} + \frac{A_{\text{Rp}} l}{1 + B_{\text{Rp}} l} \tag{4}$$

with $R_{p,0}$ (m/s), A_{Rp} (1/s) and B_{Rp} (1/m) parameters, which are dependent on the composition of the freeze-dried product, its concentration and the freezing step (Kochs et al., 1993; Searles et al., 2001; Hottot et al., 2007). These parameters are determined experimentally by fitting to experimental data.

R_p increases when l increases during the primary drying step (Eq. (13)). In order to keep T_i below the collapse temperature of the product, in most cases the energy input needs to decrease during primary drying.

The driving force for ice sublimation is the pressure difference between the water vapour pressure at the sublimation front $P_{w,i}$ and the water vapour pressure in the freeze-dryer chamber $P_{w,c}$ which can be adjusted.

$P_{w,i}$ is calculated by the following equation (Overcashier et al., 1999):

$$P_{w,i} = 2.7\,10^{10}\,\mathrm{e}^{-6145/T_i} \tag{5}$$

with T_i the product temperature at the sublimation front (K).

To optimise the drying efficiency without losing an elegant cake structure, T_i is targeted to be equal to – but not exceeding – the glass transition temperature T_g'.

In most cases, T_c is several degrees higher than T_g' as the high viscosity of the sample close to T_g' prevents viscous flow (Kasper and Friess, 2011).

The second limitation of the sublimation rate next to R_p is the

choked flow limit. Choked flow is described as a loss of pressure control due to equipment limitation, at the level of the vial neck or at the level of the duct connecting the chamber with the condenser (Patel et al., 2010). For batch freeze-drying, the duct connecting the chamber with the condenser is the most critical point where choked flow can occur. More precisely at the narrowest point of the duct, being the valve separating the drying chamber from the condenser. The gas flow through the vial neck is low due to the low sublimation rate but the freeze-dryer contains a lot of vials creating a high gas flow at the condenser duct. During continuous freeze-drying, the amount of vials being processed at the same time in the equipment is smaller but the gas flow through the vial neck is higher compared to batch freeze-drying due to the larger product surface area. Choked flow occurs once the vapour flow rate through the vial neck approaches the speed of sound, where a further increase in mass flow would result in an elevated vapour density, leading to a local pressure increase inside the vial. From the relationship between temperature at the sublimation front and the corresponding pressure, it can be deduced that a higher pressure leads to a higher temperature at the sublimation front. This temperature increase will lead to local exceeding of the product temperature and potential collapse. A safety factor of 30% is taken into account to calculate the maximal speed of the gas flow ($v_{sound,safe}$).

The choked flow condition is calculated with the following equations:

$$c = \sqrt{\frac{\gamma R T_{wv}}{M}} \tag{6}$$

$$v_{sound,safe} = 0.3c \tag{7}$$

$$V_{max} = v_{sound,safe}\pi(d_{v,o}/2)^2 \tag{8}$$

$$\dot{m}_{max} = V_{max}\rho_{wv} \tag{9}$$

with c the velocity of sound (m/s), γ the adiabatic constant for a triatomic gas (–), R the molar gas constant (J/mol K), T_{wv} the temperature of the water vapour, M the molar mass of water (kg/mol), $v_{sound,safe}$ the safe velocity of sound (m/s), V_{max} the maximum volume of sublimed gas (m^3/s), $d_{v,o}$ the diameter of the vial opening (m), $\dot{m}_{max}$ the maximum mass of sublimed gas (kg/s) and ρ_{wv} the density of the water vapour (kg/m^3).

The density of the water vapour ρ_{wv} (kg/m^3) is given by:

$$\rho_{wv} = \frac{P_{wv} M}{R T_{wv}} \tag{10}$$

with P_{wv} the water vapour pressure above the sublimation front (Pa), M the molar mass of water (kg/mol), R the molar gas constant (J/mol K) and T_{wv} the temperature of the water vapour (K).

$\dot{m}_{sub}$ (calculated by Eq. (1)) has to be compared with $\dot{m}_{max}$ to ensure the choked flow criterium is not violated. If $\dot{m}_{sub}$ would be higher than $\dot{m}_{max}$, $\dot{m}_{sub}$ is to be fixed at $\dot{m}_{max}$ in Eq. (1). Based on $\dot{m}_{sub}$ the power that should be provided to the vial to sublimate the ice (P_{sub}) (J/h) can be calculated:

$$P_{sub} = \dot{m}_{sub}\Delta H_s \tag{11}$$

with $\dot{m}_{sub}$ the sublimation rate (kg/h) and ΔH_s the latent heat of ice (J/kg).

The electric heating pad temperature to be set (T_h) corresponding to P_{sub} is given by:

$$T_h = \frac{P_{sub}}{A_p K_v} + T_v \tag{12}$$

with P_{sub} the power needed to sublimate the ice (J/h), A_p the surface area of the spin frozen product (m^2), K_v the heat transfer coefficient (J/m^2 s K) and T_v the temperature of the vial (K). The maximum temperature of the heating pad used in this study is restricted to 80 °C. This value depends on the type of heating pad. The temperature ramp of the used heating pad (18 °C/min) at the start of primary drying is taken into account.

Finally, the increase in the dried layer thickness (Δl) for a specified time interval Δt (h) is given by:

$$\frac{\Delta l}{\Delta t} = \frac{\dot{m}_{sub}}{A_p \rho_{ice} \phi} \tag{13}$$

with $\dot{m}_{sub}$ the sublimation rate (kg/h), A_p the surface area of the product (m^2), ρ_{ice} the density of ice (kg/m^3) and ϕ the volume fraction of ice (–).

These calculations are repeated for the next layer thickness (previous dry layer thickness + increase in dry layer thickness). This calculated total dry layer thickness is increasing in time and the simulation is ended when the sum of the dried layer thicknesses equals the initial layer thickness after spin freezing of the product.

R_p depends on the dry layer thickness (Eq. (4)) thus leading to an R_p which is changing in time during primary drying. This affects the maximum amount of power which can be transferred towards the product at every time step. The output of the mechanistic model is the optimal dynamic temperature profile of the electric heating pad every process minute during primary drying.

It was chosen from a practical point of view to predict the optimal dynamic temperature profile of the electric heating pad surface instead of the optimal dynamic power profile because some energy input of the heating pads is lost towards the environment and because some energy is used for heating the heating pad itself. It was impossible to quantify and model this energy loss.

Furthermore for the type of heating pad used in this study it was not possible to calibrate for the power input and the temperature output of the electric heating pad. Herewith was the by the model predicted dynamic temperature profile set under PID control. The thermocouple measured process variable is the electric heating pad temperature which is the result of the power input controlled by the PID algorithm.

3.2. K_v determination of the electric heating pad

The heat transfer coefficient between a shelf and the bottom of a vial for batch freeze-drying consists of the sum of three terms (Pisano et al., 2011):

$$K_v = K_c + K_r + K_g \tag{14}$$

with K_v the overall heat transfer coefficient between the shelf and the vial, K_c the heat transfer coefficient for the direct conduction from the shelf to the vial at the contact points, K_r the heat transfer coefficient for the radiation and K_g the heat transfer coefficient from the conduction through the gas. The same equation is used for the conductive drying with electric heating pads where K_c is the heat transfer coefficient for the direct conduction from the electric heating pad to the vial at the contact points. The heat transfer coefficient K_v of the electric heating pads to the applied vials (see further) was determined by performing different spin frozen pure ice sublimation experiments at different pressure levels (Pisano et al., 2011). A 10R vial containing 3 mL water was spin frozen and freeze-dried. Three different pressure levels were tested: 10 Pa, 20 Pa and 30 Pa. The Amsco Finn-Aqua GT4 freeze-dryer (GEA, Köln, Germany) was used as a vacuum chamber. After spin freezing, the vial was placed inside the cylinder formed by the electric heating pad within 15 ± 5s and transferred to the chamber of the freeze-dryer. The electric heating pad was installed under a pre-cooled shelf (−10 °C) to avoid contact with the shelves (Fig. 3).The energy for sublimation was provided by the electric heating pad, which was wrapped around the vial, and was also kept constant during the experiment (10 V, 0.10 A).

After 30 min of primary drying, the process was interrupted by venting the chamber with dry nitrogen gas and the mass of sublimed ice was gravimetrically determined. Based on this mass of sublimed ice and the primary drying time, the sublimation rate $\dot{m}_{sub}$ was calculated. The experiment was performed in triplicate at each pressure level. The product temperature (T_i) and heating pad temperature (T_h) were

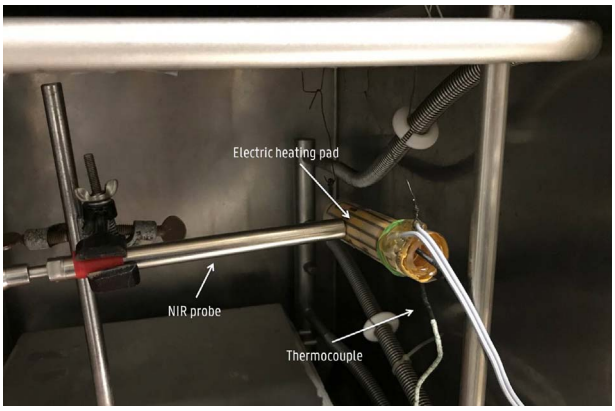

Fig. 3. Experimental setup to monitor the freeze-drying process with NIR.

monitored with Type-K thermocouples (WIKA instruments, Klingenberg, Germany) which were pressed against the ice inside the vial and against the external part of the heating pad, respectively. K_v was calculated after each experiment using the following equation:

$$K_v = \frac{\dot{m}_{sub}\Delta H_s}{A_v M(T_h - T_i)} \quad (15)$$

with $\dot{m}_{sub}$ the sublimation rate (kg/s), ΔH_s the latent heat of ice (J/kg), A_v the surface area of the vial (m^2), M the molar mass of water (kg/mol), T_h the temperature of the electric heating pad (K) and T_i the product temperature at the sublimation front (K).

To obtain the parameters describing K_v as function of P_c, nonlinear regression was used to fit the following equation to the obtained data from the above K_v experiments where K_v was plotted for the different pressure levels. The equation is adapted from literature (Koganti et al., 2011; Pikal et al., 1983; Pikal, 1985).

$$K_v = \alpha + \frac{\beta P_c}{1 + \gamma P_c} \quad (16)$$

with α (J/(m^2 s K)), β (J/(m^2 s KPa)) and γ (1/Pa) parameters describing K_v quantitatively in function of P_c.

3.3. Experimental model validation

The above developed model allowing the calculation of the dynamic heating pad settings during primary drying was applied and verified for a model formulation. The model formulation consisted of mannitol 30 mg/ml, sucrose 3.42 mg/ml, glycine 3.75 mg/ml and sodium chloride 0.58 mg/ml. Mannitol, sucrose and glycine were purchased from Sigma–Aldrich (Saint Louis, MO, USA). Sodium chloride was purchased from Fagron (Waregem, Belgium).

A 10R type I glass vial (Schott, Müllheim, Germany) was filled with 3.0 mL of the formulation and spin frozen as reported by De Meyer et al. (De Meyer et al., 2015). After spin freezing, the vial was placed inside the cylinder formed by the electric heating pad and transferred to the chamber of the freeze-dryer within 15 ± 5 s. The electric heating pad was installed under a pre-cooled shelf (−10 °C) to avoid contact with the shelves (Fig. 3). When the desired pressure level was reached (13.3 Pa), the programmed dynamic temperature profile as calculated in Section 3.1 was started. The mass of ice which already sublimed before the desired pressure level was reached is experimentally determined and the initial mass of ice is corrected by this value in the mechanistic model. The values of the input parameters used for the calculations of the dynamic temperature profile are overviewed in Table 1. The product resistance parameters were adopted from literature (Kuu et al., 2006).

The drying process was monitored with in-line NIR spectroscopy to determine the primary drying endpoint (De Meyer et al., 2015). The last temperature value of the dynamic temperature profile was maintained for 30 min to ensure that primary drying completely finished to determine the endpoint of primary drying with NIR spectroscopy. The experimental model verification was repeated six times.

3.4. NIR spectroscopy

To determine the endpoint of primary drying of the model formulation in the spin frozen vials, an NIR probe coupled to a Fourier-transform near-infrared (FT NIR) spectrometer (Thermo Fisher Scientific, Zellik, Belgium, Nicolet Antaris II near-IR analyzer) was implemented in the drying chamber of the freeze-dryer and placed against the vial through a small hole (32 mm^2) in the electric heating pad (Fig. 3).

The diffuse reflectance NIR spectra were collected in a continuous and non-invasive way during the in-line NIR experiments. The NIR spectrometer was equipped with an InGaAS detector, a quartz halogen lamp and a fiber-optic non-contact probe which was brought into the drying chamber through a vacuum feed through in the sidewall of the chamber. Spectra were taken from 10,000 cm^{-1} to 4500 cm^{-1} with a resolution of 8 cm^{-1} and averaged over 32 scans. Every process minute, a spectrum was recorded. The NIR probe was positioned in front of the hole in the electric heating pad. The sidewall of the vial was hence monitored with a spot size of about 28 mm^2. The effective sample size measured by the NIR probe hence consisted of a small part of the total sample volume (3.0 ml) but it was assumed that this part is representative for the whole product. It was from a practical point of view not possible and also not desired (since non-contact measurements are preferred) to bring the NIR probe inside the vial.

3.5. Multivariate data analysis

Principal component analysis (PCA) was applied to analyze the in-line collected NIR spectra using a multivariate data analysis software package (Simca 14.1, Umetrics AB, Umeå, Sweden). The spectra taken before activation of the electric heating pad were deleted from the dataset. The 10,000 cm^{-1} to 7500 cm^{-1} region was also excluded from the dataset since this region does not contain valuable spectral information. The spectra were preprocessed using standard normal variation (SNV) to eliminate the additive baseline offset variations and multiplicative scaling effects in the spectra (Vercruysse et al., 2014), Savitzky–Golay filtering (quadratic polynomial function fitted to moving sub-model, each containing fifteen data points) and mean centering prior to analysis.

PCA produces an orthogonal bilinear data matrix decomposition, where principal components (PCs) are obtained in a sequential way to explain maximum variance:

Table 1
Nominal values of the input parameters to calculate the dynamic temperature profile of the electric heating pads.

Parameter	Numerical value
ΔH_s	2838 J/g
M	0.018015 kg/mol
R	8.3144621 J/mol K
γ	1.33
ρ_{ice}	918 kg/m^3
ρ_{sol}	1000 kg/m^3
ϕ	1
Vial inner radius $r_{v,i}$	0.0109 m
Filling volume V	3.0 mL
Heat transfer coefficient K_v	14.94 J/m^2 s K
Product resistance parameter $R_{p,0}$	1.85 × 10^4 m/s
Product resistance parameter A_{Rp}	1.20 × 10^7 1/s
Product resistance parameter B_{Rp}	−6.76 × 10 1/m
Glass transition temperature max concentrated formulation T_g'	240.15 K

$$D = \mathrm{TP}^T + E = t_1 p_1' + t_2 p_2' + \cdots + t_Q p_Q' + E \quad (17)$$

where T is the $M \times Q$ score matrix, P the $N \times Q$ loading matrix, E the $M \times N$ model residual matrix, Q the number of PCs, N the number of collected spectra at M wavelengths. Each PC consists of two vectors, the score vector t and the loading vector p. The score vector contains a score value for each spectrum, and this value informs how the spectrum is related to the other spectra in that particular component. The loading vector indicates which spectral features in the original spectra are captured by the component studied. These unique and orthogonal PCs can be very helpful in deducing the number of different sources of variation present in the data and the occurrence of groups of related objects. However, these PCs do not necessarily correspond to the true underlying factors causing the data variation, since each PC is obtained by maximizing the amount of remaining variance (De Beer et al., 2009).

3.6. Determination of the glass transition temperature of the maximally freeze concentrated formulation T_g'

The thermal behaviour of the model formulation was evaluated via modulated differential scanning calorimetry (MDSC) using a differential scanning calorimeter (DSC) Q2000 V24.11 equipped with a RCS90 refrigerated cooling system (TA Instruments, Leatherhead, UK). Nitrogen was used as the purge gas through the DSC cell (50 ml/min) and the RCS unit (300 ml/min). Samples (± 10 mg) were run in hermetically closed standard aluminium pans supplied by TA Instruments. Mass of the sample pan and empty reference pan were taken into account. The experimental method consisted of an initial 5 min isothermal equilibration period at −90 °C. During the subsequent heating run an underlying heating rate of 2 °C/min from −90 °C to 0 °C, a modulation amplitude of 0.318 °C and a period of 60 s were applied. Temperature and enthalpic calibration was performed with an indium standard, whereas calibration of the heat capacity was performed with a sapphire standard. The experiment was replicated in triple. The glass transition temperature (T_g') was calculated as inflection point using the TA Instruments Universal Analysis 2000 V4.5A Software.

4. Results and discussion

4.1. Output primary drying model for the continuous freeze-drying process

The mechanistic primary drying model allows predicting the optimal dynamic temperature profile of the electric heating pads required for as efficient as possible primary drying of spin frozen vials without cake collapse. The calculated optimal temperature of the electric heating pad T_h is plotted in function of the primary drying time t for the studied model formulation (Fig. 4). It was experimentally determined that 0.1313×10^{-3} kg ice sublimed during the initial pressure decrease. For this reason, the dried layer thickness l does not start at zero at the start of primary drying. After 52 min 30 s of primary drying, the calculated l equals the initial total layer thickness (1.6 mm) indicating the end of primary drying. After placing the spin frozen vial in the electric heating pad, the heating pad is cooled by the in liquid nitrogen spin frozen vial. The initial T_h is −10 °C and equals the temperature of the frozen vial when the primary drying vacuum level is reached (13.3 Pa). This implicates that the product temperature exceeded T_g' during 7–8 min which possibly resulted in annealing. The optimal calculated heating pad temperature of the heating pad increases towards the maximum T_h of 80 °C at the maximal temperature ramp for this type of heating pad, being 18 °C/min. Due to the increasing R_p during primary drying, T_h gradually decreases to 30.65 °C at the end of primary drying. Hence the T_h setpoint depends on R_p. At the beginning of primary drying (after the temperature ramp up), R_p is low, hence allowing a high T_h. As primary drying progresses, R_p increases resulting in a lower allowed energy input to avoid cake collapse.

During the experimental validation it became clear that the maximum heating pad temperature of 80 °C could not be reached due to limitations of the heating pad used. The maximum reachable temperature appeared to be 50 °C. This heating pad temperature restriction is inherently coupled to a longer primary drying time being 56 min 40 s. This dynamic heating pad temperature as function of primary drying time is plotted in Fig. 5.

4.2. K_v determination of electric heating pads

The results of the K_v experiments (Table 2) revealed no significant difference in K_v (14.94 J/m^2 s K) for the different tested pressure levels.

The close contact between the electric heating pad and the entire vial wall reduces the contribution of the gas conduction (K_g) component to K_v, making this parameter independent of the chamber pressure. The radiation (K_r) component is also minimalised due to shielding of the vial by the electric heating pad. This is confirmed by the K_v determination experiments.

Since these experiments revealed that K_v is independent of P_c, P_c is fixed at 13.3 Pa in the mechanistic model. Eq. (1) defines the relation between $\dot{m}_{sub}$ and $P_{w,c}$ where the difference between $P_{w,i}$ and $P_{w,c}$ is the driving force for sublimation. To calculate the optimal dynamic heating pad temperature, within the chamber pressure range of 10–30 Pa, a pressure of 13.3 Pa was chosen as chamber pressure value in the mechanistic model. 10 Pa should provide a higher sublimation rate (driving force ($P_{w,i} - P_{w,c}$) increases) but due to the in-line NIR measurements (i.e. NIR probe interfacing in the drying chamber), the minimal reachable P_c is 13.3 Pa.

4.3. Experimental model validation

All model validation runs ($n = 6$) were continuously monitored with in-line NIR spectroscopy. PCA and interpretation was done according to the method described by De Meyer et al. (De Meyer et al., 2015). After preprocessing and PCA of the collected NIR spectra, a scores scatter plot was created for each validation run. Fig. 6 shows the scores scatter plot (PC1 versus PC2) of the first experiment. 75.5% of the spectral variation is captured in the first principle component. The second principle component covers 22.3% of the spectral variation.

All validation runs were analyzed as described below and similar trends could be seen. The scores scatter plots and loading plots of the other validation runs are not shown.

Looking at the loading line plots of PC1 and PC2 (Figs. 7 and 8 respectively), the band at 5160 cm^{-1} is facing downwards for PC1 and upwards for PC2. This band is the result of a combination of O–H stretching and H–O–H bending vibrations of water (Pieters et al., 2012).

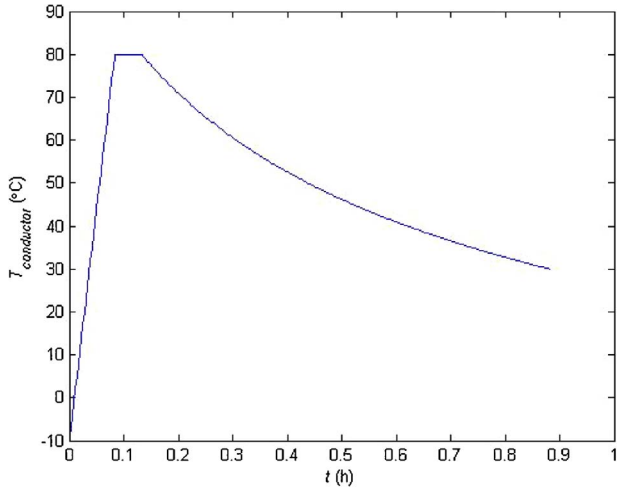

Fig. 4. Dynamic heating pad temperature T_h as function of primary drying time t. The heating pad temperature was restricted to 80 °C.

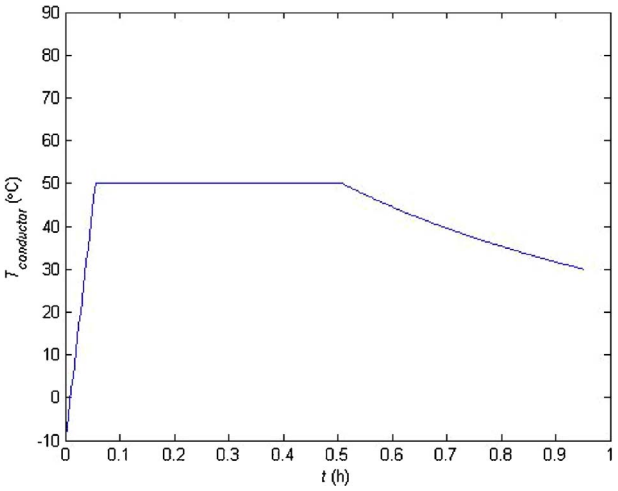

Fig. 5. Dynamic heating pad temperature T_h as function of primary drying time t. The heating pad temperature was restricted to 50 °C.

Table 2
Experimentally determined K_v values at three different pressure levels for a 10R vial surrounded by an electric heating pad.

Chamber pressure (Pa)	K_v (J/m^2 s K)	SD (J/m^2 s K)
10	14.75	1.30
20	14.97	0.99
30	15.09	1.03

A broad band can be noticed between 5500 cm^{-1} and 7000 cm^{-1} with a maximum at 6700 cm^{-1} which is typical for ice in the formulation. It originates from symmetric and asymmetric stretch of ice. This band faces downwards in PC1 and upwards in PC2. Scores moving in the positive direction along PC1 and the negative direction of PC2 indicate the removal of ice from the formulation.

The loadings of these PCs indicate that the trajectory of the score plot originates from changes in the ice and water content in the formulation during the freeze-drying process, allowing the determination of the primary and secondary drying endpoint (De Meyer et al., 2015).

In depth analysis of the scores scatter plot reveals that at the start of primary drying the scores are clustered, indicating there were no changes in the spectra during the start of primary drying. Only the overwhelming ice bands are visible in the NIR spectra (Fig. 9a). Ice

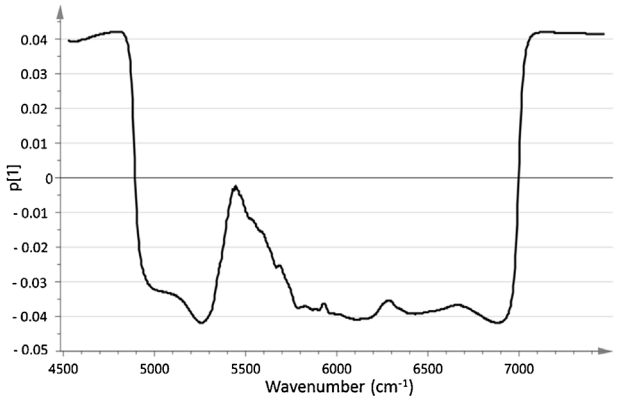

Fig. 7. Loading line plot of PC1.

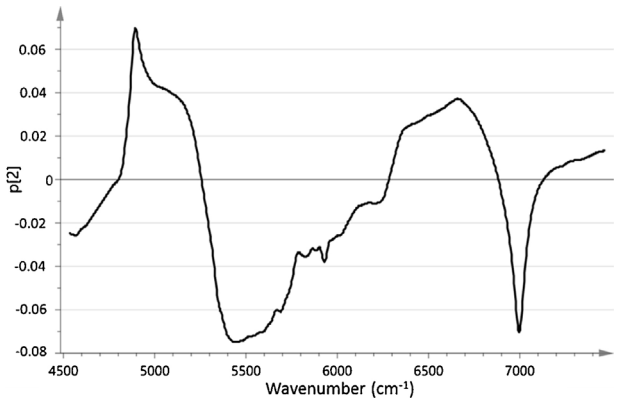

Fig. 8. Loading line plot of PC2.

sublimation occurs at this moment but as sublimation starts at the top of the frozen product layer (i.e. on the inner side of the vial) this is not detected by the NIR probe which is positioned at the outside of the vial.

After 18 min of primary drying, the scores start moving in a positive direction on the PC2 axis. The intensity of the NIR bands around 5160 cm^{-1} and 6700 cm^{-1} starts to increase (Fig. 9a). This is confirmed by the loading line plot of PC2 where both bands are faced upwards. This could be explained by the decreasing ice layer thickness and the fact that the sublimation front is moving towards the NIR probe. The NIR light only has a limited penetration depth and the ice signals overwhelm the spectra until the decreasing ice layer thickness

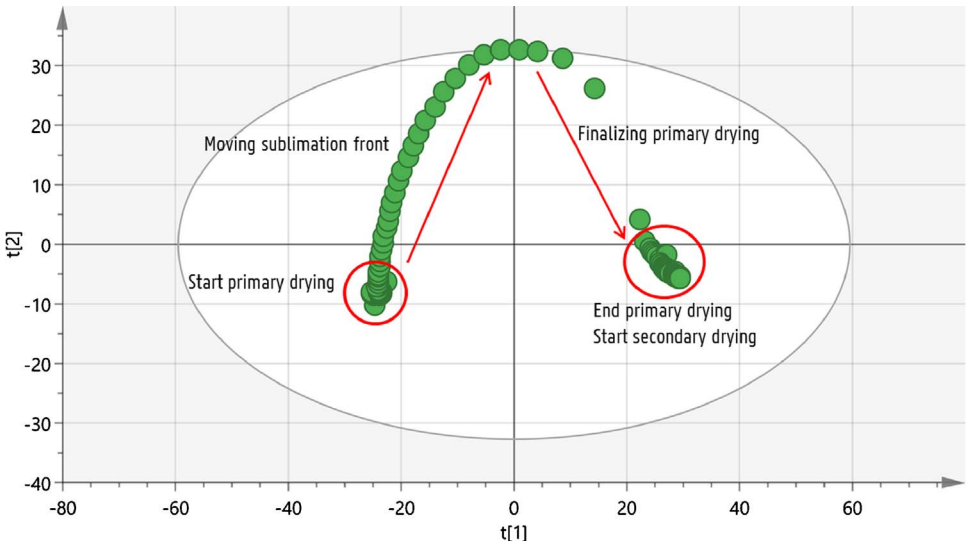

Fig. 6. Scores scatter plot after principle component analysis of the first verification experiment.

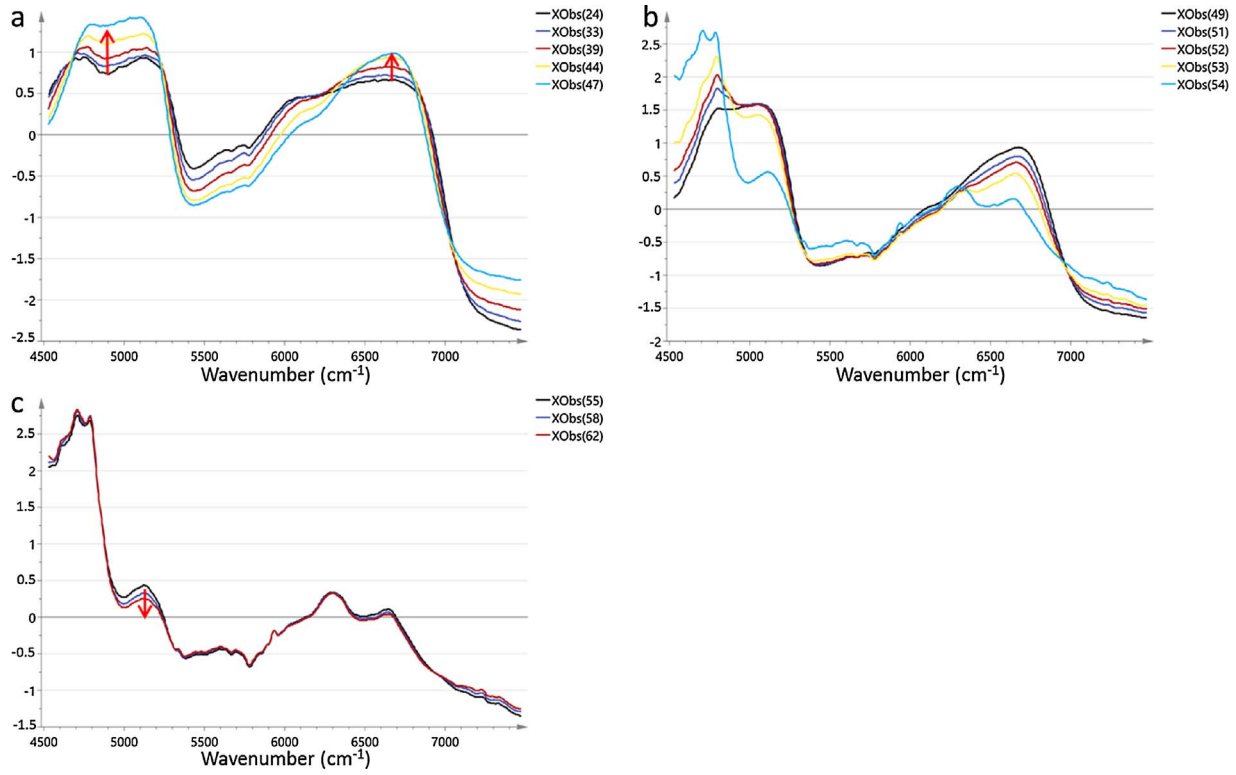

Fig. 9. Visualization of the primary drying process based on in-line collected NIR spectra: (a) primary drying progress: overwhelming ice bands during first part of primary drying. (b) Formulation characteristic NIR bands appear in the spectra. Primary drying ends when the last ice signal disappears. (c) Secondary drying: water band at 5160 cm^{-1} decreases in intensity.

allowed the detection of underlying water and formulation-characteristic excipient bands.

At the first inflection point, the primary drying had progressed to such an extent that the sublimation front was within sight of the NIR probe, and the water band and characteristic excipient bands appear in the spectra. Ice bands are still visible in the spectra but their intensity is reduced (Fig. 9b).

Between the inflection point and the second cluster of scores, the primary drying process is finalizing. The scores move in a negative direction along PC2 and a positive direction along PC1. The ice bands in the loading plot of PC2 are facing upwards and downwards in PC1 so this movement along PC1 and PC2 indicates the complete removal of ice.

The second cluster formed by the scores indicates the endpoint of primary drying. Secondary drying starts during the finalization of primary drying and is visualized by a decrease of the free water band at 5160 cm^{-1} (Fig. 9c) (De Meyer et al., 2015; Pieters et al., 2012).

The primary drying endpoint was determined for every verification run and the ratio between this experimental determined primary drying endpoint and the model-based primary drying endpoint (56 min 40 s) was made. The results of this comparison can be found in Table 3. The mean ratio was 1.05 ± 0.07, indicating a good agreement between the experimental and computed primary drying time.

The small mismatch between the experimental and model based primary drying endpoints could be explained by (i) at the NIR monitoring site, a hole in the electric heating pad is created leading to a possible different energy transfer at that location (ii) some assumptions and simplifications were introduced in the mechanistic model ($P_{w,c}$ assumed to be equal to P_c, 30% safety factor for choked flow (see Section 3.1)) (iii) some input parameters in the model are estimations or experimentally determined values associated with an error (e.g. K_v, T_g').

All six verification runs resulted in a freeze-dried product with an elegant cake aspect without any visual signs of cake collapse (Fig. 10).

5. General conclusion and future perspectives

The developed mechanistic model allows calculating the optimal dynamic heating pad temperature during primary drying of spin frozen formulation in vials. Experimental data revealed that K_v is independent of the chamber pressure. Based on in-line NIR monitoring, the endpoint of primary drying for the verification experiments was determined and compared to the model predicted primary drying endpoint. These verification experiments showed a good agreement between both endpoints (1.05 ± 0.07). The visual aspect of the freeze-dried formulation was good without any visual signs of macroscopic cake collapse. An uncertainty analysis will be conducted in the future to explore the influence of the estimated input variables and process parameters on the model output. Similar to this research, Van Bockstal et al. described the development of a mechanistic model to determine the dynamic infrared heater temperature during primary drying in a continuous freeze-drying process (Van Bockstal, 2017). The results of the uncertainty analysis on that mechanistic model will be compared to the results of the uncertainty analysis of the mechanistic model developed in this paper.

Table 3
Relation between the experimental primary drying time and the model based primary drying time (56 min 40 s) for the different validation runs.

Experiment	Experimental primary drying time (min)	Ratio experimental vs model based primary drying time (–)
1	64	1.13
2	55	0.97
3	62	1.09
4	59	1.04
5	54	0.95
6	62	1.09

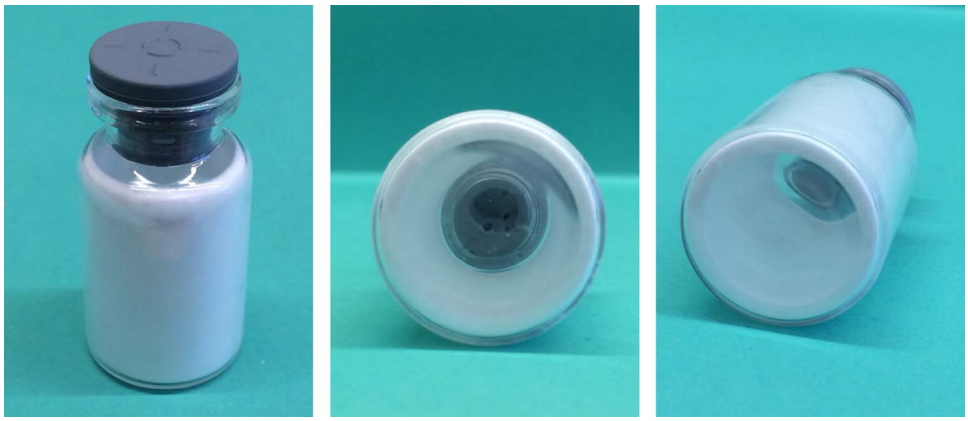

Fig. 10. Visual aspect of the freeze-dried formulation obtained with the settings of the validation run.

References

FDA, C., 2016. Novel Drugs Summary (January 2017).

Chi, E.Y., Krishnan, S., Randolph, T.W., Carpenter, J.F., 2003. Physical stability of proteins in aqueous solution: mechanism and driving forces in nonnative protein aggregation. Pharm. Res. 20.

Costantino, H., Pikal, M., 2004. Lyophilization of Biopharmaceuticals.

De Meyer, L., Van Bockstal, P.J., Corver, J., Vervaet, C., Remon, J.P., De Beer, T., 2015. Evaluation of spin freezing versus conventional freezing as part of a continuous pharmaceutical freeze-drying concept for unit doses. Int. J. Pharm. 496.

Wang, W., 2000. Lyophilisation and Development of Solid Pharmaceuticals 203.

Pikal, M.J., Shah, S., Senior, D., Lang, J.E., 1983. Physical chemistry of freeze-drying: measurement of sublimation rates for frozen aqueous solutions by a microbalance technique. J. Pharm. Sci. 72.

Rey, L., May, J.C., 2010. Freeze Drying/Lyophilization of Pharmaceutical and Biological Products 206.

Jennings, T., 1999. Lyophilization: Introduction and Basic Principles 25.

Kasper, J.K., Friess, W., 2011. The freezing step in lyophilization: physico-chemical fundamentals, freezing methods and consequences on process performance and quality attributes of biopharmaceuticals. Eur. J. Pharm. Biopharm. 78.

Pikal, M.J., 2002. Freeze drying. Encyclopedia of Pharmaceutical Technology, 3rd ed. .

Sarragua, M.C., De Beer, T., Vervaet, C., Remon, J.P., Lopes, J.A., 2010. A batch modelling approach to monitor a freeze-drying process using in-line Raman spectroscopy. Talanta 83.

Kauppinen, A., Toiviainen, M., Korhonen, O., Aaltonen, J., Paaso, J., Juuti, M., Ketolainen, J., 2013. In-line multipoint near-infrared spectroscopy for moisture content quantification during freeze-drying. Anal. Chem. 85.

Corver, J., 2013. Method and system for freeze-drying injectable compositions. Particular Pharmaceutical.

Van Bockstal, P.-J., De Meyer, L., Corver, J., Vervaet, C., De Beer, T., 2017. Noncontact infrared-mediated heat transfer during continuous freeze-drying of unit doses. J. Pharm. Sci. 106, 71–82.

Van Bockstal, P.J., 2017. Mechanistic modelling of infrared mediated energy transfer during the primary drying step of continuous freeze-drying process. Eur. J. Pharm. Biopharm. 114.

Koganti, V.R., Shalaev, E.Y., Berry, M.R., Osterberg, T., Youssef, M., Hiebert, D.N., Kanka, F.A., Nolan, M., Barrett, R., Scalzo, G., Fitzpatrick, G., Fitzgibbon, N., Luthra, S., Zhang, L., 2011. Investigation of design space for freeze-drying: use of modeling for primary drying segment of a freeze-drying cycle. AAPS PharmSciTech 12.

Mortier, S.T.F.C., Van Bockstal, P.J., Corver, J., Nopens, I., Gernaey, K.V., De Beer, T., 2016. Uncertainty analysis as essential step in the establishment of the dynamic design space of primary drying during freeze-drying. Eur. J. Pharm. Biopharm. 103.

Konstantinidis, A.K., Kuu, W., Otten, L., Nail, S.L., Sever, R.R., 2011. Controlled nucleation in freeze-drying: effects on pore size in the dried product layer, mass transfer resistance, and primary drying rate. J. Pharm. Sci. 100.

Fissore, D., Pisano, R., Barresi, A.A., 2011. Advanced approach to build a design space for the primary drying of a pharmaceutical freeze-drying process. Int. J. Drug Dev. Res. 100 (11), 4922–4933.

Fissore, D., Pisano, R., Velardi, S., Barresi, A., Galan, M., 2009. PAT tools for the optimization of the freeze-drying process. Pharm. Eng. 29.

Kochs, M., Körber, C., Heschel, I., Nunner, B., 1993. The influence of the freezing process on vapour transport during sublimation in vacuum-freeze-drying of macroscopic samples. Int. J. Heat Mass Transf. 36.

Searles, J.A., Carpenter, J.F., Randolph, T.W., 2001. The ice nucleation temperature determines the primary drying rate of lyophilization for samples frozen on a temperature-controlled shelf. J. Pharm. Sci. 90.

Hottot, A., Vessot, S., Andrieu, J., 2007. Freeze drying of pharmaceuticals in vials: influence of freezing protocol and sample configuration on ice morphology and freeze-dried cake texture. Chem. Eng. Process. Process Intensif. 46.

Overcashier, D.E., Patapoff, T.W., Hsu, C.C., 1999. Lyophilization of protein formulations in vials: investigation of the relationship between resistance to vapor flow during primary drying and small-scale product collapse. J. Pharm. Sci. 88.

Patel, S.M., Doen, T., Pikal, M.J., 2010. Determination of end point of primary drying in freeze-drying process control. AAPS PharmSciTech 11.

Pisano, R., Fissore, D., Barresi, A.A., Chimica, I., Torino, P., 2011. Heat Transfer in Freeze-Drying Apparatus.

Pikal, M., 1985. Use of laboratory data in freeze drying process design: heat and mass transfer coefficients and the computer simulation of freeze drying. J. Parenter. Sci. Technol. 39.

Kuu, W.Y., Hardwick, L.M., Akers, M.J., 2006. Rapid determination of dry layer mass transfer resistance for various pharmaceutical formulations during primary drying using product temperature profiles. Int. J. Pharm. 313.

Vercruysse, J., Toiviainen, M., Fonteyne, M., Helkimo, N., Ketolainen, J., Juuti, M., Delaet, U., van Assche, I., Remon, J., Vervaet, C., De Beer, T., 2014. Visualization and understanding of the granulation liquid mixing and distribution during continuous twin screw granulation using NIR chemical imaging. Eur. J. Pharm. Biopharm. 86.

De Beer, T., Vercruysse, P., Burggraeve, A., Quinten, T., Ouyang, J., Zhang, X., Vervaet, C., Remon, J.P., Baeyens, W.R.G., 2009. In-line and real-time process monitoring of a freeze-drying process using Raman and NIR spectroscopy as complementary process analytical technology (PAT) tools. J. Pharm. Sci. 98.

Pieters, S., De Beer, T., Kasper, J.C., Boulpaep, D., Waszkiewicz, O., Goodarzi, M., Tistaert, C., Friess, W., Remon, J.P., Vervaet, C., Vander Heyden, Y., 2012. Near-infrared spectroscopy for in-line monitoring of protein unfolding and its interactions with lyoprotectants during freeze-drying. Anal. Chem. 84.